MRI near metal objects: Investigating the effects of induced RF currents and currents induced by gradient switching on SE phase images using a simple model system

H. Wojtczyk[1], P. Martirosian[1], V. Ballweg[1], H. Graf[1], and F. Schick[1]
[1]Section on Experimental Radiology, University Hospital Tuebingen, Tuebingen, Baden-Wuerttemberg, Germany

Introduction/Objective Interest in MR imaging near embedded metal objects has increased in recent years due to the growing number of metallic implants and interventional MRI procedures. So far, much research has focused on susceptibility-related encoding difficulties and their mitigation [1]. However, electrical currents induced in the metals by RF pulses or by gradient switching play an important role, too. Both types of current are known to cause artifacts in SE magnitude images [2-4], and SE phase images have also been shown to be affected by induced currents [5]: While inhomogeneities of the static magnetic field are compensated for, SE phase images may be influenced by transient magnetic field inhomogeneities, such as those caused by induced currents. The objective of the present study was to systematically assess for the first time which effects both types of current have on SE phase images, using a simple model system. In a flat conductive sheet in the coronal plane, as has been examined here, electrical currents can be induced by a change of the y-component of the magnetic flux density, i.e. dB_y/dt. This can either be caused by a RF pulse or by the switching of the imaging gradient fields G_y and G_z, which are accompanied by concomitant (parasitary) gradient fields in the y-direction [6]. Imaging parameters have been varied in a way that is expected to be able to separate the effects of both types of current: Induced RF currents are expected to be affected by a reduction of the transmit voltage, whereas the currents induced by gradient switching are expected to be influenced by the choice of the encoding directions, the bandwidth and the position of the sheet inside the MR scanner.

Material and Methods A copper sheet (100 mm x 15 mm, 3 mm thick) was arranged in a box containing 3.8 l of Gd-doped water ($T_1 \approx 40$ ms) such that the sheet lay perpendicular to $\mathbf{B_0}$ and in the center of the x-z-plane. Imaging was performed in a sagittal slice at the center of the copper sheet using the body coil of a 1.5 T scanner (Siemens Healthcare, Erlangen, Germany). A SE sequence was employed (FoV 256x256 mm^2, slice thickness 3 mm, matrix 256x256, TR = 200 ms, TE = 20 ms, 6 averages; the varied parameters are listed in tab. 1). The phase images were subject to post-processing: A shift of the background phase was accomplished using MATLAB (The MathWorks, Natick, MA, USA).

Tab. 1: Parameters for the SE measurements (position in the y- and z-direction, phase encoding direction, readout gradient, bandwidth and transmit voltage).

No.	y	z	PED	G_{read}	BW	U_{Trans}
a	- 60 mm	0 mm	H>>F	G_y	781 Hz/Px	Auto
b	- 60 mm	0 mm	A>>P	G_z	201 Hz/Px	Auto
c	- 60 mm	0 mm	A>>P	G_z	501 Hz/Px	Auto
d	- 60 mm	0 mm	A>>P	G_z	651 Hz/Px	Auto
e	- 60 mm	0 mm	A>>P	G_z	781 Hz/Px	Auto
f	- 60 mm	0 mm	A>>P	G_z	781 Hz/Px	Auto/2
g	0 mm	0 mm	H>>F	G_y	781 Hz/Px	Auto
h	0 mm	0 mm	A>>P	G_z	781 Hz/Px	Auto
i	0 mm	0 mm	A>>P	G_z	781 Hz/Px	Auto/2
j	0 mm	60 mm	H>>F	G_y	781 Hz/Px	Auto

Results The resulting MR images are presented in fig. 1a-j. Most of the SE phase images showed artifacts that varied considerably in shape and intensity depending on the measurement parameters: A pronounced four-leaved artifact pattern was visible for y = - 60 mm, $G_{read} = G_z$ and high bandwidths (esp. fig. 1e) as well as for z = 60 mm and $G_{read} = G_y$ (fig. 1j), while a six-leaved artifact pattern occurred for z = 0 mm and $G_{read} = G_y$ (fig. 1 a,g). In contrast, there were no distinct artifacts present for y = - 60 mm, $G_{read} = G_z$ and small bandwidths (esp. fig. 1b) as well as for y = z = 0 mm (i.e. in the isocenter) and $G_{read} = G_z$ (fig. 1h). The reduction of the transmit voltage did not have a significant effect on the phase image apart from decreasing the SNR (see fig. 1e-f).

Discussion/Conclusions Although induced RF currents were clearly present on the copper sheet (see the bright regions next to the sheet in the magnitude image in fig. 1i, which was acquired using a reduced transmit voltage), for the measurements performed here the SE phase images were dominated by effects from currents induced by gradient switching. Assuming that the B_y-component of the concomitant fields has a gradient in the y- and in the z-direction for G_z and G_y, respectively (see [6]), uncompensated eddy currents according to fig. 2a-b could be induced by the switching of the readout gradient, depending on the readout direction and on the position of the copper sheet. These two current patterns produce transient magnetic field inhomogeneities whose z-component $B_{ind,z}$ in a sagittal plane was calculated (see fig. 1k-l) using Mathematica (Wolfram Research, Champaign, IL, USA). The simulations are in good qualitative agreement with the artifact patterns observed in the SE phase images. Note that according to this model, no current is induced by the switching of the readout gradient for y = z = 0 mm (i.e. when the sheet is located in the isocenter) and $G_{read} = G_z$ (see fig. 1h). SE phase imaging is a sensitive and powerful tool suitable for the investigation of currents induced by gradient switching. Potential applications of this method include the visualization and evaluation of eddy current paths on metallic implants, the localization of instruments in interventional MRI procedures as well as conductivity measurements. Further theoretical and experimental research is required to elucidate whether induced RF currents can have any effect on SE phase images at all and if so, whether SE phase imaging can be utilized to quantify these currents. This would be desirable as induced RF currents pose a major security risk for MRI near metal objects.

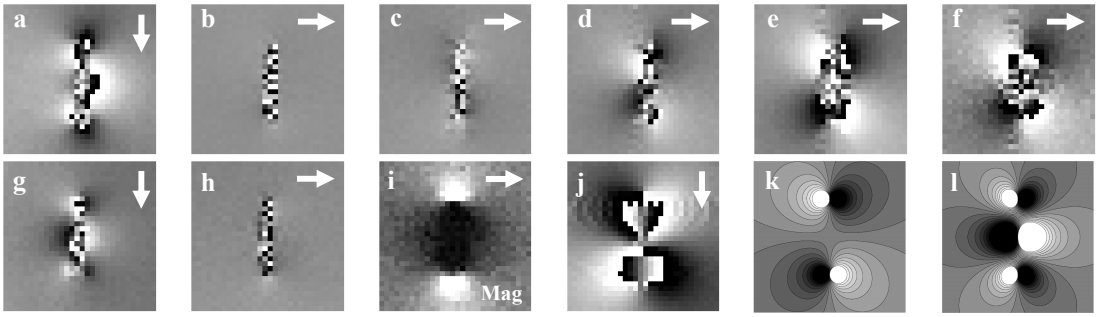

Fig. 1: a-j: SE phase (a-h,j) and magnitude (i) images (3x3 cm^2) of the copper sheet (images correspond to the measurement details specified in tab. 1; the white arrows indicate the PED); k-l: calculated contour plots of the $B_{ind,z}$-component corresponding to the current patterns depicted in fig. 2a-b.

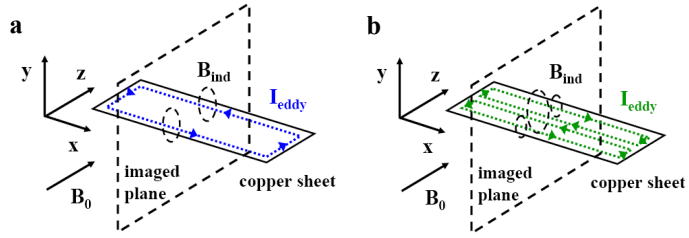

Fig. 2: Schematic of the assumed eddy current patterns on the copper sheet. a: one current loop (blue) along the border of the sheet (assumed for y = - 60 mm and $G_{read} = G_z$ as well as for z = 60 mm and $G_{read} = G_y$); b: two opposing current loops (green) in the two halves of the sheet (assumed for z = 0 mm and $G_{read} = G_y$).

References [1] Koch KM et al., JMRI 32:773-87 (2010) [2] Camacho CR et al., JMRI 5:75-88 (1995) [3] Shenhav A et al., MRM 52:1465–8 (2004) [4] Graf H et al., MRM 54:231–4 (2005) [5] Graf H et al., Med Phys 33:124-7 (2006) [6] Norris DG et al., MRI 8:33-7 (1990)